

**NATIONAL ADVISORY COMMITTEE  
FOR AERONAUTICS**

TECHNICAL NOTE

**MAR 1, 1947**

No. 1214

PERFORMANCE OF A RADIAL-INLET IMPELLER DESIGNED  
ON THE BASIS OF TWO-DIMENSIONAL-FLOW THEORY  
FOR AN INFINITE NUMBER OF BLADES

By I. A. Johnsen, W. K. Ritter  
and R. J. Anderson

Aircraft Engine Research Laboratory  
Cleveland, Ohio



Washington  
March 1947

**NACA LIBRARY**  
LANGLEY MEMORIAL AERONAUTICAL  
LABORATORY  
Langley Field, Va.





3 1176 01433 8967

NATIONAL ADVISORY COMMITTEE FOR AERONAUTICS

TECHNICAL NOTE NO. 1214

PERFORMANCE OF A RADIAL-INLET IMPELLER DESIGNED  
ON THE BASIS OF TWO-DIMENSIONAL-FLOW THEORY

FOR AN INFINITE NUMBER OF BLADES

By I. A. Johnsen, W. K. Ritter  
and R. J. Anderson

SUMMARY

A radial-inlet impeller based on two-dimensional-flow theory has been investigated in a research program to establish correlation between flow theory and impeller performance. The simplifying assumptions of an infinite number of blades and an incompressible fluid were made for this impeller design. The blade shape was determined by imposing a predetermined vortex distribution that was chosen to relieve the loading in the critical regions of the impeller passage. The performance of the impeller was experimentally obtained in a variable-component test unit in conjunction with a vaneless diffuser of NACA design. An analysis of flow characteristics in the compressor, using static-pressure experimental data and the assumption of an infinite number of blades, indicated that the peak impeller efficiency was high and that the low over-all efficiency could be largely attributed to losses in the vaneless diffuser. The entrance section of the impeller and the passage in the region of the impeller-blade tip operated ineffectively even at the point of peak over-all efficiency. The entrance loss, which became very large at high flow, was the principal factor determining the form of the compressor-performance curve. The method developed for determining compressor performance from static-pressure measurements is limited to radial-inlet-type impellers in which flow is essentially two dimensional.

INTRODUCTION

One of the principal obstacles in the development of efficient centrifugal compressors has been the lack of a sound mathematical basis for the design of the impeller and the analysis of impeller-channel flow. Adverse pressure gradients are generally recognized

as producing flow separation in the impeller passage, which results in large losses. No method exists by which these adverse pressure gradients can be predetermined and controlled under conditions of three-dimensional flow, such as exists in the passages of conventional centrifugal impellers. Furthermore, the determination of actual pressures existing in the passages of modern centrifugal-type impellers would require extremely difficult instrumentation, and no comprehensive pressure surveys in such passages have been obtained.

In a research program to establish correlation between flow theory and impeller performance, a two-dimensional radial-inlet impeller was selected as a first approach. This type of impeller allowed a performance analysis based on readily obtainable measurements and the use of existing flow theory. Methods have been presented (references 1 and 2) for the study of two-dimensional flow by use of conformal transformation. The method of conformal transformation presented in reference 2 can be directly applied to impeller design and has the advantage of being applicable to a wide range of design assumptions. This method was used in the design of the research impeller.

The impeller was designed by using the simplest concepts of two-dimensional flow: an infinite number of blades and an incompressible fluid. This procedure permitted the tentative establishment of the limitations of the infinite-blade theory as a basis for impeller design. The impeller-blade shape was determined by imposing a predetermined vortex distribution that was chosen to relieve the loading in the critical regions of the impeller passage. This choice of vortex distribution was arbitrary and experimental verification will be required for the choice of the optimum distribution.

The performance of a compressor composed of the radial-inlet impeller and a vaneless diffuser was investigated using data obtained in a variable-component test setup. In addition to the standard over-all compressor-performance ratings, the characteristics of flow in the impeller and diffuser passages were determined. This analysis of flow, which was based on readily available static-pressure measurements, was possible because of the two-dimensional nature of the flow through the impeller. This experimental determination of performance using static-pressure data was a valuable phase of the development program because it indicated required modifications to the basic design theory. Inasmuch as the program was essentially an impeller investigation, the diffuser performance was not extensively investigated.

## IMPELLER DESIGN

The design of the impeller-blade shape followed the method suggested in reference 2 in which infinitesimal portions of the blades are replaced by vortices that are periodically distributed on a circle. This vortex strength follows a prescribed distribution that is summed up along the radius to determine the blade shape. This initial radial-inlet impeller was designed to reduce the loading in the entrance and exit regions of the impeller by the choice of a semielliptical graph of vortex distribution against radius; that is, the vortex distribution at design flow is zero at the entrance and the discharge tip of the blade. The details of the blade shape calculated by this method are given in appendix A.

Based on these considerations, the 18-blade radial-inlet impeller shown in figure 1 was constructed by the NACA. Because the blades are nonradial at most points in the impeller, they are subject to a blade-bending stress under the action of centrifugal force. The blade stresses were analytically investigated and the blade cross section chosen was one that would give reasonable blade stresses under the impeller operating conditions.

The radial-inlet impeller differs from conventional impellers in that the velocity of the air at the impeller entrance is radial. Inasmuch as an axial inlet pipe was used, this radial velocity was provided by a flared section that changed the direction of flow from an axial to a radial direction. A mock-up of the inlet section was made to investigate the velocity distribution at a station corresponding to the entrance edges of the blades. The velocity variation across this station over an air-flow range comparable with that encountered in compressor tests is shown in figure 2 in terms of  $V/V_{av}$ , the ratio of the local air velocity to the average air velocity at the station. These inlet mock-up studies indicated that the entrance velocity distribution was satisfactory for the full range of compressor air flow.

## EXPERIMENTAL SETUP

The radial-inlet impeller was initially investigated in a variable-component test setup similar to the one described in reference 3. The impeller was tested with a 34-inch vaneless diffuser of NACA design that has a passage-area divergence equivalent to a cone with an apex angle of  $60^\circ$  and lying along the ideal logarithmic spiral flow path for design flow. This type of diffuser gives a flat performance curve.

The location of standard instruments and the precision of instrumentation were those recommended in reference 4, except that the inlet measuring station was 4 instead of 2 pipe diameters from the impeller-inlet plane. In addition to the standard instrumentation, static-pressure taps were installed along the impeller stationary front shroud and the front and rear diffuser walls. The accuracy of static-pressure survey readings was  $\pm 0.05$  inch of mercury.

The impeller was operated in accordance with the procedures of reference 4 at actual tip speeds from 800 to 1300 feet per second. At each speed, the flow was varied from wide-open throttle to the incipient surge point of the unit. Inlet air was inducted directly from the test cell; the inlet-air temperature varied from  $76^{\circ}$  to  $83^{\circ}$  F during the investigation. A compressor lampblack flow pattern was made at the peak efficiency point at an actual tip speed of 1200 feet per second.

## RESULTS AND DISCUSSION

### Performance Characteristics Based on Standard

#### Over-all Measurements

The over-all compressor characteristics (adiabatic efficiency  $\eta_{ad}$ ; total-pressure ratio  $p_{t,2}/p_{t,1}$ ; corrected volume flow  $Q_{t,1}/\sqrt{\theta}$ , and corrected tip speed  $U/\sqrt{\theta}$ ) were calculated according to the standard procedures of references 4 and 5. Details of the calculated parameters and the defined symbols are given in appendix B.

The over-all total-pressure-ratio characteristics of the radial-inlet impeller tested with the vaneless diffuser are shown in figure 3 for corrected tip speeds from 782 to 1279 feet per second. Contour plots of adiabatic efficiency are superimposed on the total-pressure-ratio curves. Because of the large losses in the vaneless diffuser, peak over-all efficiencies for the complete assembly of impeller, diffuser, and collector were rather low, varying from 0.705 at a corrected tip speed of 782 feet per second to 0.625 at a corrected tip speed of 1279 feet per second.

## Performance Characteristics Based on Static-Pressure Measurements

The variation in static pressure through the impeller and the diffuser provides an initial indication of the location and relative magnitude of losses in the compressor. On the basis of these static-pressure values plus calculated kinetic-energy values, an analysis of the flow characteristics in the compressor may be made. This analysis is made for the peak-efficiency-flow point over a range of tip speeds and for a range of flows at an actual tip speed of 800 feet per second. Details of the method of calculating compressor performance using static-pressure data are given in appendix B.

Static-pressure variation. - The variation in static pressure through the impeller and the diffuser is shown in figure 4 for maximum, minimum, and one intermediate air flow and for the flow at peak over-all efficiency at actual tip speeds of 800, 1000, and 1200 feet per second. These static-pressure profiles are shown as a ratio of the local static pressure  $p_s$  to the inlet-pipe static pressure  $p_{s,1}$ . For operation at other than the design flow, the condition existing at the entrance section of the impeller is the principal factor determining the static-pressure profile and the operation of the impeller. Under conditions where an extreme angle of attack exists at the entrance edge of the impeller blade, a loss in static pressure occurs in the region of the impeller entrance. This primary pressure loss, which is never recovered, results in a secondary loss because it is multiplied by the pressure ratio through the impeller. The primary loss may be considered to be analogous to a pressure drop in improperly designed inlet elbows of a supercharger installation.

Peak-efficiency operation. - The radial distribution of the addition of energy was analyzed for the flow points of peak over-all efficiency by determining useful and total work of compression by means of the static-pressure calculation method of appendix B. The curves of the useful work of compression based on the assumption that air follows the curvature of the impeller channel  $H_{ad,c}$  and the total work of compression based on the same assumption  $H_c$  for the peak-efficiency points at actual tip speeds of 800, 1000, and 1200 feet per second (fig. 5), which have a marked similarity over the tip-speed range, show the rate of addition of energy in the system. The location and the magnitude of the principal losses

can be estimated from the relative slopes of  $H_c$  and  $H_{ad,c}$ . In the impeller, the main losses occur in the entrance section and in the region of the impeller tip. The portion of the work done in these ineffective regions is, however, reduced because of the reduction of loading resulting from the vortex distribution used in the design.

The losses in the diffuser are large at all speeds, as indicated by the drop in  $H_{ad,c}$  from the impeller tip to the diffuser discharge. No extensive study was made of the losses in the diffuser because the program was basically an impeller investigation, but a large part of the losses apparently occurred near the inner radius. A lampblack flow pattern obtained at the peak-efficiency point for a tip speed of 1200 feet per second showed no evidence of separation on the diffuser surfaces.

The local-operating-efficiency term  $\eta_l$ , as developed in appendix B, gives an indication of the efficiency at which each portion of the impeller is operating. Curves of this local operating efficiency for the peak-efficiency points at actual tip speeds of 800, 1000, and 1200 feet per second (fig. 6) substantiate the conclusion that the entrance section of the impeller operates ineffectively. As discussed in appendix B, this low efficiency may represent either a direct pressure loss or a partly recoverable potential loss. In either case, however, the operation in the entrance portion of the impeller departs appreciably from ideal conditions. The local operating efficiency increases with radius until in the region between the 4.5- and the 6-inch radius the impeller operates at an efficiency approaching 1.00. Beyond the 6-inch radius, the efficiency falls off to a value of approximately 0.65 at the 7-inch radius. This apparent drop in efficiency may be due to an undervaluation of the kinetic energy, which is possibly the result of a separation caused by the preceding sharp bend in the impeller passage.

The magnitude of the various losses and the effect of tip speed on efficiency are shown in figure 7. The calculated values for the peak adiabatic compressor efficiency  $\eta_{ad,c}$  from the impeller entrance to the impeller tip and to the diffuser exit are shown with the over-all peak efficiency  $\eta_{ad}$  based on the standard analysis of references 4 and 5. The peak impeller efficiency is high, ranging from 0.90 to 0.86 over the tip-speed range from 800 to 1300 feet per second. The drop in efficiency through the diffuser is large, with the drop increasing at higher tip speeds

to a maximum of 20 points at 1300 feet per second. The drop in efficiency resulting from losses in the collector and in the inlet and outlet pipes was relatively small and the drop remained very nearly constant throughout the speed range.

The determination of  $H_c$  and  $H_{ad,c}$  is dependent on the assumption that air follows the curvature of the channel. Although this assumption provides a method of analyzing the flow in the impeller, it results in an overvaluation of both  $H_c$  and  $H_{ad,c}$ . A more precise evaluation of the tangential velocity of the air at the discharge tip and of the work of compression of the entire impeller may be made using the measured value of total temperature in the outlet pipe of the lagged installation. An adiabatic efficiency term  $\eta_{ad,o}$ , using these values of tangential air velocity at the discharge tip and the total work of compression of the impeller, may be determined by a static-pressure analysis method similar to that developed in appendix B for determining the energy terms. This analysis, although it cannot be applied to stations within the impeller, provides a measure of compressor performance at the impeller discharge tip. The efficiency of compression from the impeller entrance to the impeller tip determined by the static-pressure analysis using outlet-pipe total temperature measurements  $\eta_{ad,o}$  shows close agreement with that determined in the analysis in which air is assumed to follow the curvature of the channel  $\eta_{ad,c}$  (fig. 7).

Operation over flow range. - Operation of the compressor unit over the full flow range was analyzed at a tip speed of 800 feet per second. The variation in  $H_c$  and  $H_{ad,c}$  for selected operating points (including maximum and minimum flow) is shown in figure 8.

At the ideal flow, the relative direction of the air is parallel to a tangent to the impeller blade at entrance. Calculations for flows greater than this value show an instantaneous drop in  $H_c$  across the blade entrance (fig. 8(a) at the maximum flow of 4030 cu ft/min) resulting from the assumption that the air-flow direction changes instantaneously to follow the impeller-blade curvature. In other words, relative to the rotating impeller, the tangential velocity of the air increases instantaneously at the impeller entrance, which by equation (2) in appendix B results in a negative value of  $H_c$ . The inlet tips of the impeller are acting as a turbine under these conditions.

The static pressure (fig. 4(a)) and therefore the useful work input (fig. 8(a)) drop off gradually rather than instantaneously, however, because the air does not make the change in direction instantaneously, as assumed in the calculation. This pressure loss, which is due to the extreme angle of attack at the entrance edge of the impeller blade, is essentially a throttling loss.

Inasmuch as the assumption that air follows the impeller blades is invalid under the extreme operating conditions at the maximum-flow point, the analysis is useful only in indicating trends at these large flows. For example,  $H_c$  appears to be less than  $H_{ad,c}$  (an impossible condition) because the air does not instantaneously change direction to follow the channel curvature. The indicated increase in  $H_{ad,c}$  in the diffuser is probably the result of inaccurate static-pressure readings in the turbulent region of the impeller tip. The calculation at the maximum-flow point definitely shows, however, that the pressure drop at the impeller entrance, which is never recovered, is the principal determining factor of the low efficiency of the unit at high load coefficients.

The same general characteristics are evident at the lower flow of 3546 cubic feet per minute (fig. 8(b)), although the magnitude of the throttling action across the impeller entrance is smaller for this flow and does not extend over so large a portion of the impeller. Here again, efficient pressure conversion begins at a point well within the impeller.

At the peak-efficiency point (fig. 5(a)), no such loss occurs in the entrance section of the impeller. The principal determining factor of the efficiency of operation of the unit therefore seems to be the condition across the impeller entrance. The curves for the minimum-flow of 1448 cubic feet per minute (fig. 8(c)) have the same general characteristics as those for the peak-efficiency point (fig. 5(a)), although the over-all efficiency of operation is slightly less.

A plot of the characteristic efficiencies over the flow range at an actual tip speed of 800 feet per second is shown in figure 9. The drop in efficiency through the diffuser is nearly constant over the principal portion of the flow range; whereas, the drop in efficiency through the pipes and in the collector increases with an increase in flow. The efficiency from the impeller entrance to the impeller tip determined from a static-pressure analysis based on total-temperature measurements in the outlet pipe  $\eta_{ad,o}$  is also shown in figure 9. A close correlation between the two methods of static-pressure analysis is again indicated.

### Hydraulic-Efficiency Characteristics

The hydraulic efficiency  $\eta_h$ , as defined in appendix B, represents the degree to which the design condition that air followed the impeller-channel curvature was approached. The hydraulic efficiency for the radial-inlet impeller at an actual tip speed of 800 feet per second (fig. 10) shows that the impeller performance approached but did not attain the performance for an impeller with an infinite number of blades. The design method based on an infinite number of blades therefore was not entirely valid. No appreciable variation in the hydraulic efficiency over the tip-speed range was indicated.

The hydraulic-efficiency characteristic for a conventional, radial-bladed impeller is presented in figure 10 for comparison with the hydraulic efficiency of the radial-inlet impeller. The curves show a marked similarity in trend and magnitude and indicate that, in the radial-inlet impeller, the deviation of the air from tangency with the impeller blade at discharge is comparable with that of conventional radial-bladed impellers.

### SUMMARY OF RESULTS

From an investigation of a compressor unit composed of a radial-inlet impeller and a vaneless diffuser by standard performance tests and by an analysis based on static-pressure measurements, the following results were obtained:

1. The over-all efficiency of the compressor was low; peak values varied from 0.705 at a corrected tip speed of 782 feet per second to 0.625 at a tip speed of 1279 feet per second. This low efficiency can be largely attributed to high losses in the 34-inch vaneless diffuser.

2. The static-pressure investigation for the peak-efficiency points shows that the entrance section of the impeller and the passage in the region of the impeller tip operated ineffectively and the section of the impeller from 4.5- to 6.0-inch radius operated at an efficiency approaching 1.00. This low operating efficiency in the entrance and discharge regions of the impeller represents either direct pressure losses or a channel that is not flowing full, either of which is detrimental to good impeller operation. The portion of the work done in these ineffective regions is, however, reduced because of reduction of loading resulting from the vortex distribution for this initial design.

The impeller efficiency determined at the impeller discharge tip is therefore high, ranging from 0.90 at an actual tip speed of 800 feet per second to 0.86 at 1300 feet per second.

3. The impeller has inherently critical entrance conditions, which induce a drop in static and total pressure in the entrance section of the impeller passage for flows greater than that at the design point. This entrance loss, which becomes very large at the maximum flow point, is never recovered and is the principal determining factor of the form of the compressor performance curve.

Aircraft Engine Research Laboratory,  
National Advisory Committee for Aeronautics,  
Cleveland, Ohio, October 16, 1946.

## APPENDIX A

## CALCULATION OF IMPELLER-BLADE SHAPE

The impeller-blade shape is determined by the method suggested in reference 2, in which infinitesimal portions of the blades are replaced by vortices that are periodically distributed on a circle. The velocities produced by the summation of these vortices are given by the following relations presented in reference 2 (the notation of reference 2 has been maintained):

$$\begin{aligned}
 rv_{\varphi} &= \frac{n}{2\pi} \int_{r_1}^r \frac{\partial \Gamma}{\partial R} \left[ 1 + \sum_{\lambda=1}^{\infty} \left( \frac{r}{R} \right)^{-\lambda n} \cos \lambda n (\varphi - \theta) \right] dR \\
 &\quad - \frac{n}{2\pi} \int_r^{r_a} \frac{\partial \Gamma}{\partial R} \sum_{\lambda=1}^{\infty} \left( \frac{r}{R} \right)^{\lambda n} \cos \lambda n (\varphi - \theta) dR \\
 rv_r &= - \frac{n}{2\pi} \int_{r_1}^r \frac{\partial \Gamma}{\partial R} \sum_{\lambda=1}^{\infty} \left( \frac{r}{R} \right)^{-\lambda n} \sin \lambda n (\varphi - \theta) dR \\
 &\quad - \frac{n}{2\pi} \int_r^{r_a} \frac{\partial \Gamma}{\partial R} \sum_{\lambda=1}^{\infty} \left( \frac{r}{R} \right)^{\lambda n} \sin \lambda n (\varphi - \theta) dR
 \end{aligned}$$

where

$r, \varphi$  polar coordinates used to describe flow

$r, \theta$  polar coordinates used to describe blade shape

$v_{\varphi}$  tangential component of air velocity

$n$  number of blades

$r_1$  radius at entrance of impeller blades

$\Gamma$  vortex strength

- R      radius of circle on which vortices are distributed  
 $r_a$     radius at discharge tip of impeller blades  
 $v_r$     radial component of air velocity

A solution can be obtained for an impeller with a finite number of blades by making a summation of these equations for the radial and tangential velocities. With the simple hypothesis of an infinite number of blades, however, the radial component of velocity vanishes and the tangential-velocity equation becomes

$$rv_\phi = \frac{n}{2\pi} \int_{r_1}^r \frac{\partial \Gamma}{\partial R} dR$$

The relation between  $\partial \Gamma / \partial R$  and  $dR$  is determined by the assumed vortex distribution. For an infinite number of blades the relative path of the fluid is coincident with the blade shape and the equation of reference 1 may be expressed as

$$\tan \phi = \frac{\frac{n}{2\pi r} \Gamma - \omega r}{v_r}$$

where

- $\phi$       angle of blade with respect to radius  
 $\omega$       angular velocity of impeller

The shape of the impeller blade can then be found by integration:

$$\phi(r) - \phi(r_1) = \int_{r_1}^r \frac{\tan \phi}{r} dr$$

The blade shape calculated by this method is shown in figure 11.

The additional assumption of an incompressible fluid and a constant radial velocity were made for this design. The impeller-blade height was calculated to give this constant radial velocity for an incompressible flow.

## APPENDIX B

## CALCULATION OF PERFORMANCE

## Symbols

The following symbols are used in the determination of compressor performance:

- A      total annular area of impeller passage at given radius,  
         sq ft
- $c_p$     specific heat of normal air at constant pressure,  
         Btu/(lb)(°F) (0.243)
- $g$       acceleration of gravity, ft/sec<sup>2</sup> (32.174)
- H      total work of compression determined from inlet- and outlet-  
         pipe measurements; increase in enthalpy per unit mass,  
         ft-lb/lb mass
- $H_{ad}$    useful work of compression determined from inlet- and outlet-  
         pipe measurements; isentropic increase in total enthalpy  
         per unit mass for given pressure rise, ft-lb/lb mass
- $H_c$     total work of compression based on assumption that all air  
         follows curvature of channel; increase in total enthalpy  
         per unit mass, ft-lb/lb mass
- $H_{ad,c}$  useful work of compression based on assumption that air  
         follows curvature of channel; isentropic increase in  
         total enthalpy per unit mass for given pressure rise,  
         ft-lb/lb mass
- J      mechanical equivalent of heat, ft-lb/Btu (778)
- $k = \frac{W}{A \cos \beta \cos \epsilon}$
- p      pressure, lb/sq ft absolute
- Q      volume flow rate, cu ft/min
- r      compressor radius, ft

T	absolute temperature, °R
U	impeller tip speed, ft/sec
V	absolute velocity of air, ft/sec
v	velocity of air relative to impeller, ft/sec
W	weight flow rate, lb/sec
$\alpha$	projected angle of mean flow line with respect to plane normal to axis of impeller rotation, deg
$\beta$	true angle of mean flow line with respect to plane normal to axis, deg ( $\tan^{-1} \cos \epsilon \tan \alpha$ ; vector diagram of relations shown in fig. 12)
$\gamma$	ratio of specific heats for normal air (1.3947)
$\epsilon$	angle of blade with respect to radius, deg
$\eta_{ad}$	over-all adiabatic efficiency determined from inlet- and outlet-pipe measurements
$\eta_{ad,c}$	adiabatic compressor efficiency based on assumption that air follows curvature of channel
$\eta_l$	local operating efficiency
$\eta_h$	hydraulic efficiency
$\theta$	ratio of actual inlet stagnation temperature to standard sea-level temperature, 518.4
$\rho$	density, lb/cu ft
$\tau$	applied torque, ft-lb
$\omega$	angular velocity of impeller, radians/sec

The subscripts denote the following:

- 1 condition at measuring station in inlet pipe
- 2 condition at measuring station in outlet pipe

- 3 condition at entrance to impeller blades
- a axial component
- r radial component
- s static, or true, stream value
- t total, or stagnation, value
- $\theta$  tangential component

### Performance Characteristics Based on Standard

#### Over-all Measurements

The over-all compressor characteristics were calculated in accordance with the standard procedures of references 4 and 5. Calculated parameters included over-all adiabatic efficiency  $\eta_{ad} = H_{ad}/H$ , total-pressure ratio  $p_{t,2}/p_{t,1}$ , volume flow corrected to standard sea-level conditions  $Q_{t,1}/\sqrt{\theta}$ , and corrected tip speed  $U/\sqrt{\theta}$ .

### Performance Characteristics Based on

#### Static-Pressure Measurements

The determination of compressor flow characteristics was based on static-pressure measurements. In the impeller, the kinetic energy was calculated from mass flow by using static-pressure measurements and assuming full flow in the impeller channel. The efficiency of operation thus determined throughout the impeller channel indicates the degree to which impeller performance approaches the design condition and indicates the regions of the impeller that should be modified for improved performance. This method of experimental analysis is limited to impellers in which flow is essentially two dimensional.

The diffuser flow characteristics were determined in a manner similar to that used in the impeller. The kinetic energy in the diffuser was calculated from mass flow and conservation of angular momentum by using static-pressure measurements and assuming full flow in the diffuser channel.

Energy terms. - The analysis of the performance of a radial-inlet impeller is made on the basis of static-pressure measurements and fundamental physical relations. A basic assumption, justified by the design assumption of an infinite number of blades, is made that flow follows the blade and fills the passage. The average state of the air at any point in the system is determined by the front-shroud static-pressure measurements, Bernoulli's equation for compressible flow, and the continuity equation. Although the front shroud is a curvilinear surface, a basic assumption of no axial variation in pressure at a given radial station can reasonably be adopted.

The energy terms  $H_c$  and  $H_{ad,c}$  referred to the state point at the impeller entrance were determined for the various compressor stations, by use of the preceding relations. The derivation of the equations for calculating these energy terms is as follows:

The energy at the impeller entrance is

$$\frac{\gamma}{(\gamma - 1)} \frac{p_{s,3}}{\rho_{s,3}} + \frac{v_3^2}{2g} = c_p T_{t,3} \quad (1)$$

The energy added by the impeller is

$$H_c = \tau\omega = \frac{\omega r v_\theta}{g} = \frac{\omega r}{g} (\omega r - v_\theta) \quad (2)$$

The energy at any point in the impeller is

$$\frac{\gamma}{(\gamma - 1)} \frac{p_s}{\rho_s} + \frac{v^2}{2g} \quad (3)$$

where

$$v^2 = v_r^2 + v_a^2 + (\omega r - v_\theta)^2$$

When the energy terms of equations (1) and (2) are equated with equation (3)

$$\frac{\gamma}{\gamma - 1} \frac{p_s}{\rho_s} - c_p T_{t,3} = \frac{\omega^2 r^2}{2g} - \frac{v^2}{2g} \quad (4)$$

From continuity of flow

$$v = \frac{W}{\rho_s A \cos \beta \cos \epsilon} = \frac{k}{\rho_s} \quad (5)$$

The following quadratic expression in terms of  $\rho_s$  is evolved by combining equations (4) and (5):

$$\rho_s^2 \left( \frac{\omega^2 r^2}{2g} + c_{p, \text{IT}, 3} \right) - \rho_s \left[ \frac{\gamma p_s}{(\gamma - 1)} \right] - \frac{k^2}{2g} = 0 \quad (6)$$

After equation (6) is solved for  $\rho_s$ , and  $v$  is determined from equation (5)

$$v_n = v \sin \beta$$

$$v_\theta = v \sin \epsilon \cos \beta$$

$$v_r = v \cos \epsilon \cos \beta$$

The total pressure is then determined from the relation

$$\frac{\gamma}{(\gamma - 1)} \frac{p_t}{\rho_t} = \frac{\gamma}{(\gamma - 1)} \frac{p_s}{\rho_s} + \frac{v^2}{2g} \quad (7)$$

By the adiabatic relation,

$$\rho_t = \rho_s \left( \frac{p_t}{p_s} \right)^{\frac{1}{\gamma}} \quad (8)$$

and, when substituted in equation (7), equation (8) gives

$$p_t = p_s \left( \frac{\gamma - 1}{\gamma} \frac{v^2}{2g} \frac{\rho_s}{p_s} + 1.0 \right)^{\frac{\gamma}{\gamma - 1}} \quad (9)$$

The useful work input to the air  $H_{ad, c}$  is calculated as the isentropic increase in total enthalpy per pound of air.

$$H_{ad,c} = c_p J T_{t,3} \left[ \left( \frac{p_t}{p_{t,3}} \right)^{\frac{\gamma-1}{\gamma}} - 1.0 \right] \quad (10)$$

The total work input per pound of air, when no prerotation of the air is assumed, is given by equation (2).

In a similar manner, the value of  $H_{ad,c}$  at any point in the diffuser passage can be determined. The total work input  $H_c$  at any point in the diffuser is taken as that at the impeller tip.

Adiabatic compressor efficiency. - The adiabatic compressor efficiency  $\eta_{ad,c}$  was determined by using calculated energy values. This term is the ratio of the useful work to the total work input, with the change of state measured from the impeller entrance to the particular compressor station:

$$\eta_{ad,c} = \frac{H_{ad,c}}{H_c}$$

Local operating efficiency in impeller. - In order to obtain an indication of the efficiency at which each portion of the impeller was operating and to locate the sources of losses in the impeller, the local operating efficiency  $\eta_l$  was expressed as

$$\eta_l = \frac{\frac{d}{dr} H_{ad,c}}{\frac{d}{dr} H_c}$$

This local-efficiency parameter is the ratio of the rate of addition of useful work to the rate of work input. This parameter was determined by graphical methods from the values of  $H_c$  and  $H_{ad,c}$  calculated by equations (2) and (10), respectively.

As a result of the assumption of full channel flow, however, regions of low local efficiency may not necessarily mean direct losses in total pressure; that is, in the event that the channel does not flow full and that a small region of high velocity exists in the impeller passage, the calculated kinetic energy and therefore the efficiency will be lower than the actual value, even though no real loss in total energy at the point of measurement

necessarily occurs. Subsequent losses (potential losses) occur, however, in the conversion of this extra kinetic energy to pressure because of the resulting turbulence in the stream; therefore, even though low local efficiencies may mean either direct losses or potential losses in energy, they indicate the region of and the approximate magnitude of the departure from design performance.

### Hydraulic Efficiency

The hydraulic efficiency  $\eta_h$  for the impeller was defined as the ratio of the actual work input to the work input that would exist under the design assumptions of full channel flow and that the air followed the curvature of the channel

$$\eta_h = \frac{H}{H_c}$$

This term is comparable with the slip factor of a conventional radial-bladed impeller but takes into account the backward slope of the blades at the discharge tip. Hydraulic efficiency represents the degree to which the design condition that air followed the impeller-channel curvature was approached.

### REFERENCES

1. Bollay, William: The Theory of Flow through Centrifugal Pumps. Theodore von Kármán Anniversary Vol., Contributions to Appl. Mech. and Related Subjects, C.I.T., May 11, 1941, pp. 273-284.
2. Betz, A., and Flügge-Lotz, I.: Design of Centrifugal Impeller Blades. NACA TM No. 902, 1939.
3. Ellerbrock, Herman H., Jr., and Goldstein, Arthur W.: Principles and Methods of Rating and Testing Centrifugal Superchargers. NACA ARR, Feb. 1942.
4. NACA Subcommittee on Supercharger Compressors: Standard Procedures for Rating and Testing Centrifugal Compressors. NACA ARR No. E5F13, 1945.
5. NACA Subcommittee on Supercharger Compressors: Standard Method of Graphical Presentation of Centrifugal Compressor Performance. NACA ARR No. E5F13a, 1945.





NACA  
C-8671  
2-21-45

Figure 1. - Radial-inlet impeller.



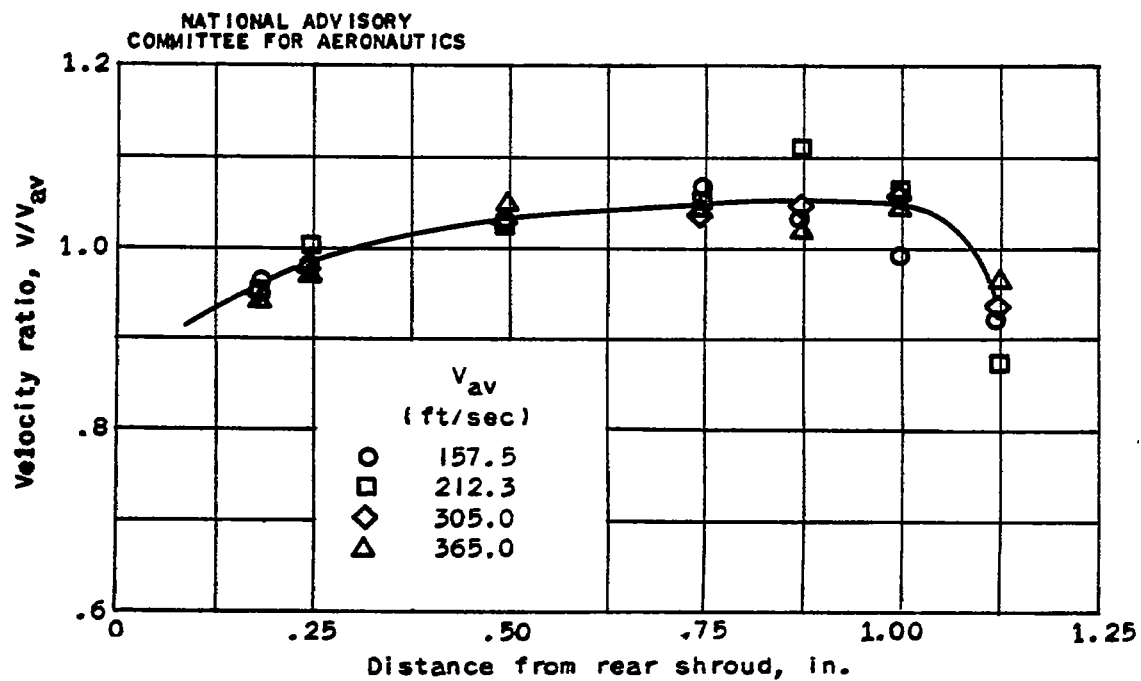


Figure 2. - Velocity profile across impeller-blade entrance section at radius of 3.5 inches as determined from mock-up tests.

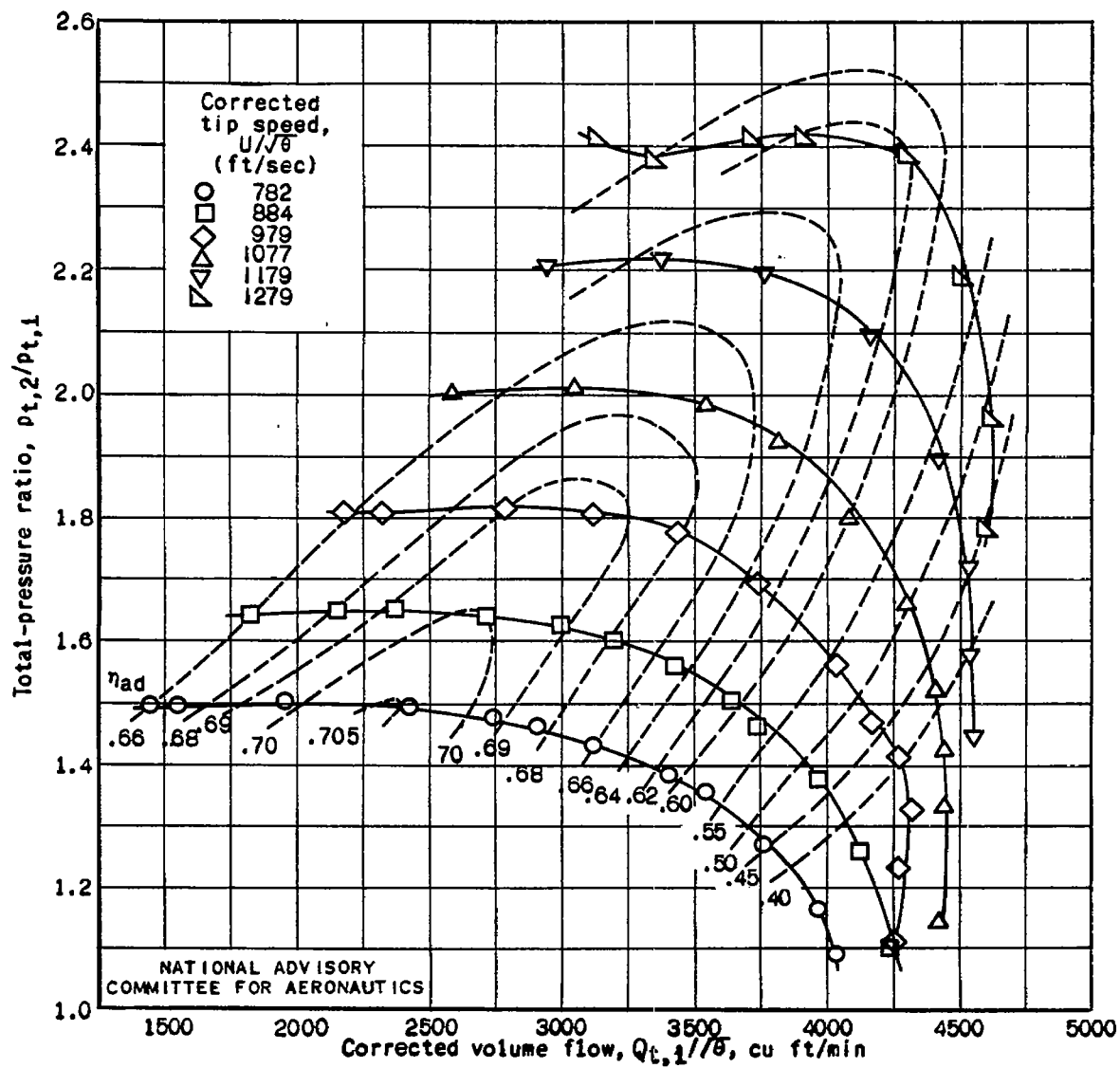
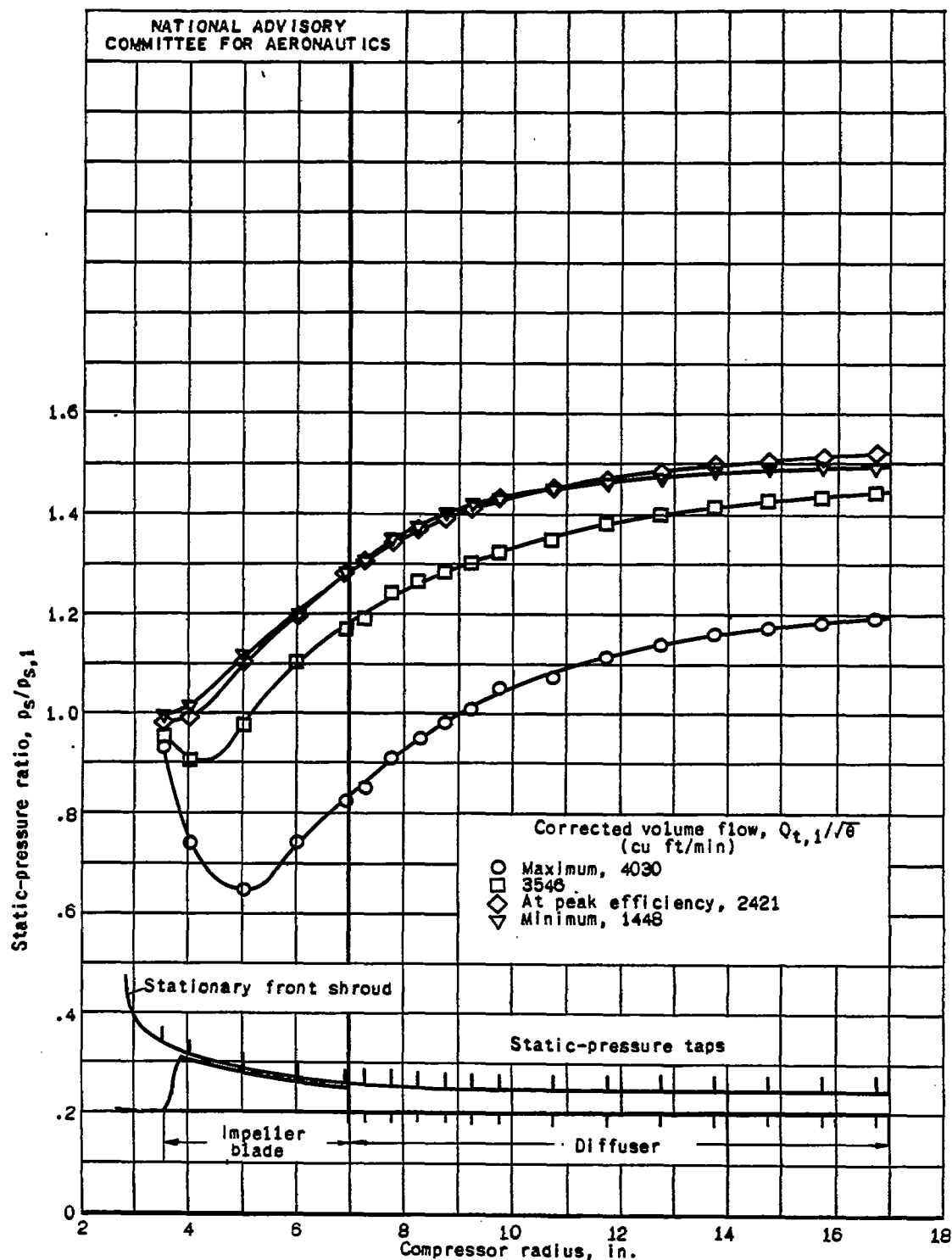


Figure 3. - Over-all total-pressure-ratio characteristics of radial-inlet impeller and vaneless diffuser.



(a) Actual tip speed, 800 feet per second.

Figure 4. - Distribution of static-pressure ratio along radius of radial-inlet impeller and vaneless diffuser.

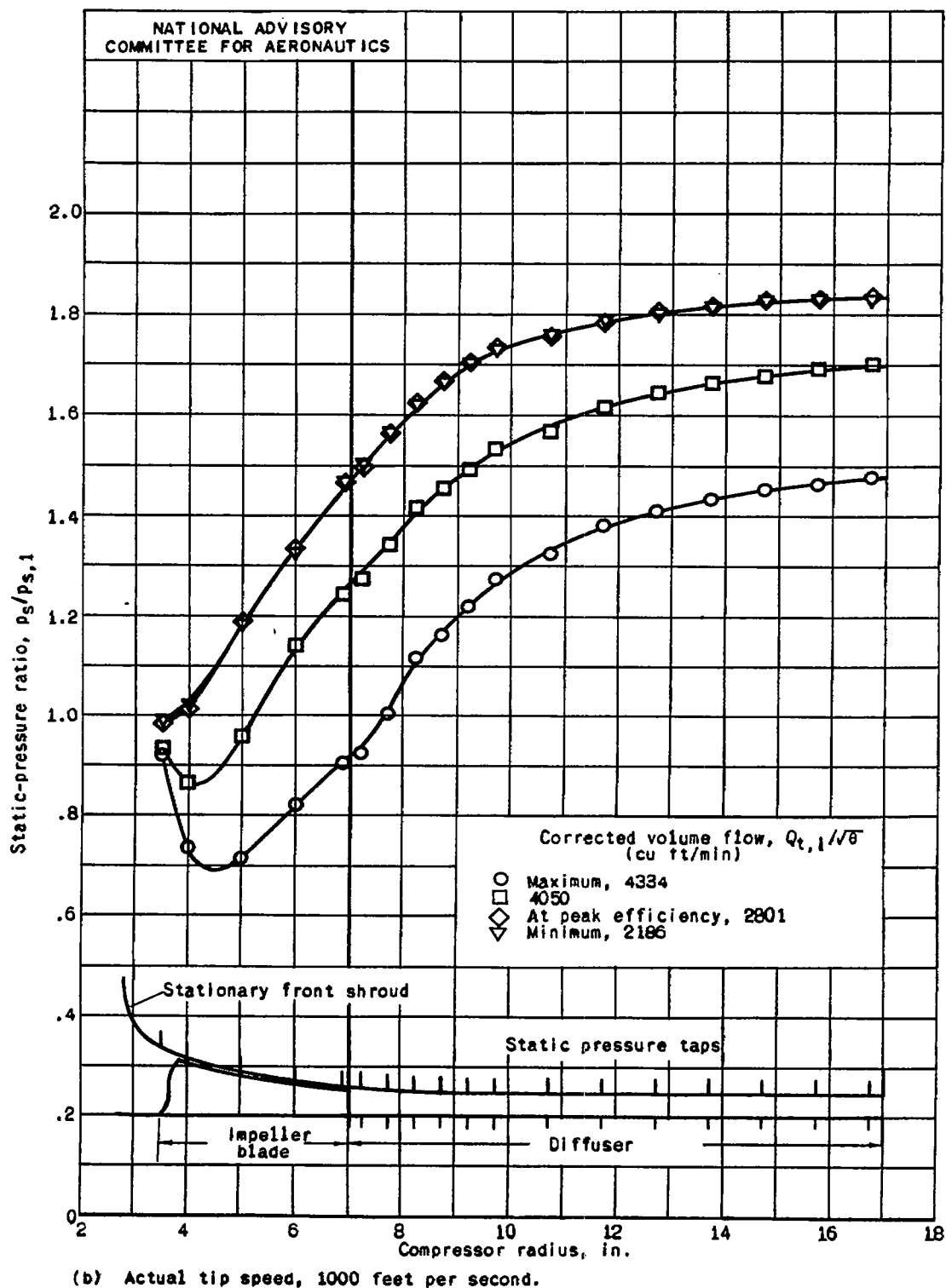
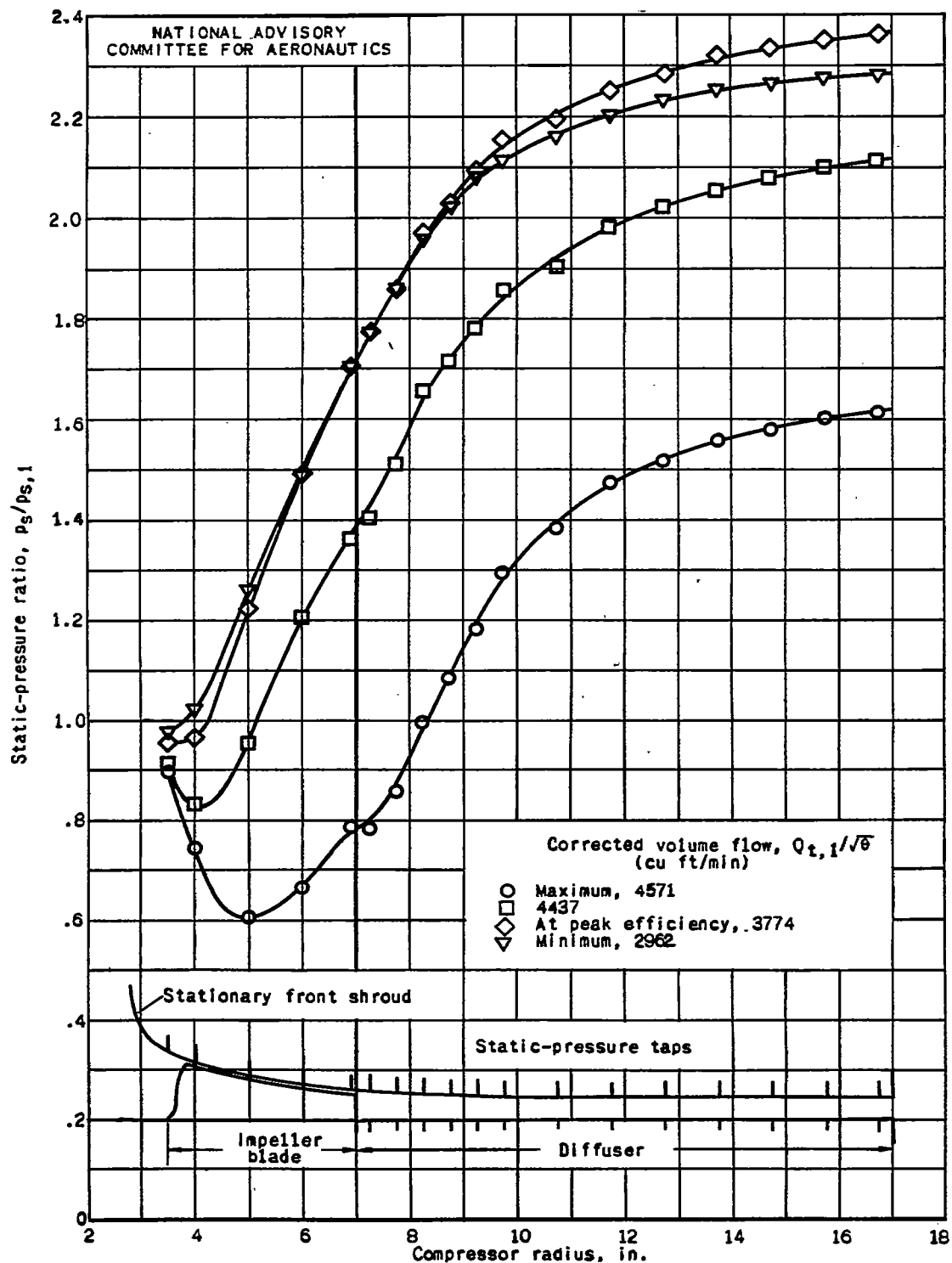


Figure 4. - Continued. Distribution of static-pressure ratio along radius of radial-inlet impeller and vaneless diffuser.

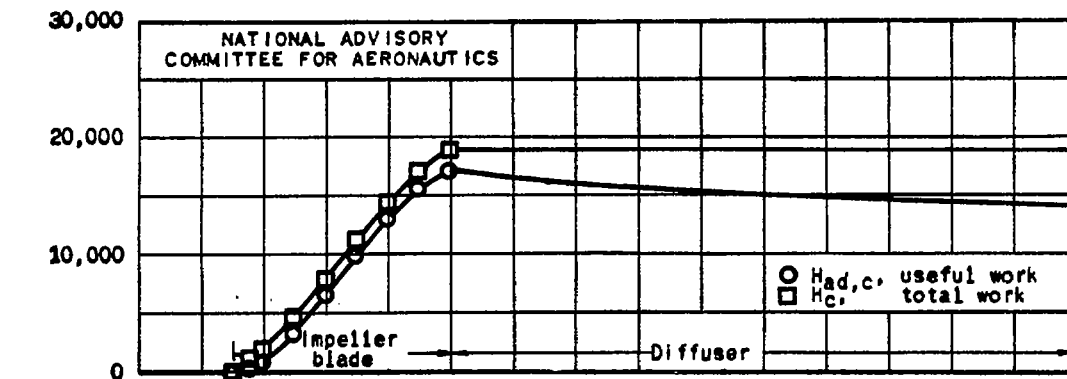


(c) Actual tip speed, 1200 feet per second.

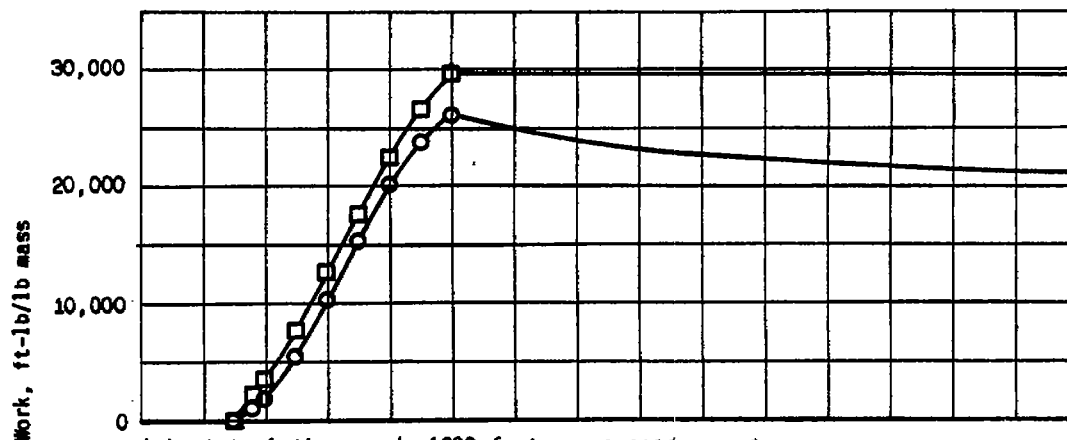
Figure 4. - Concluded. Distribution of static-pressure ratio along radius of radial-inlet impeller and vaneless diffuser.

Fig. 5

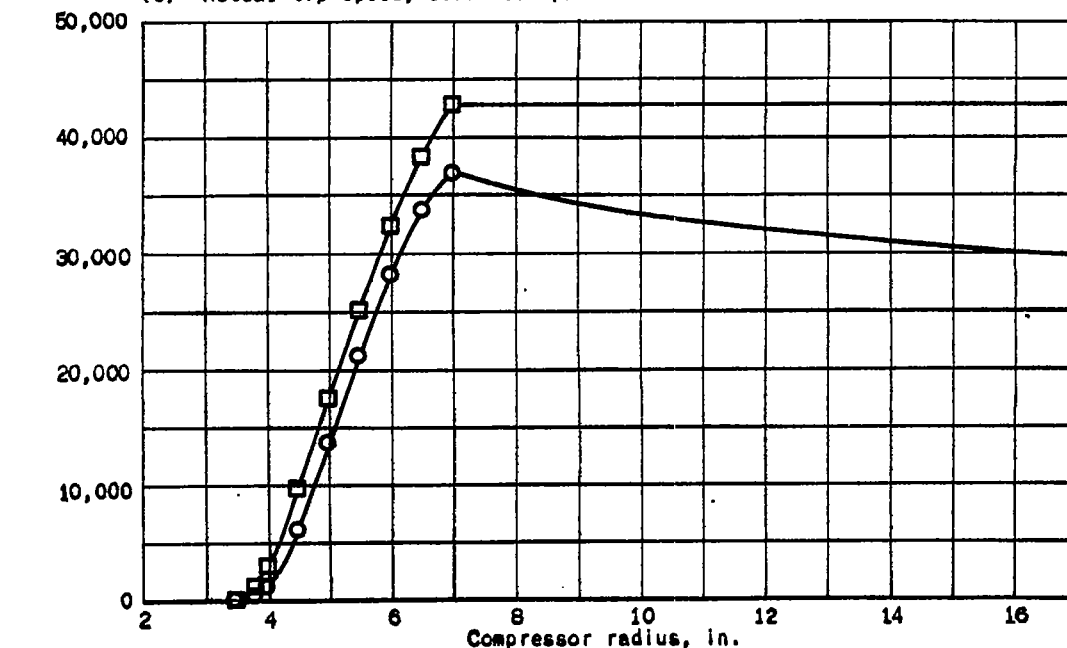
NACA TN No. 1214



(a) Actual tip speed, 800 feet per second.



(b) Actual tip speed, 1000 feet per second.



(c) Actual tip speed, 1200 feet per second.

Figure 5. - Distribution of useful work  $H_{ad,c}$  and total work  $H_c$  of compression along radius of radial-inlet impeller and vaneless diffuser at peak-efficiency points.

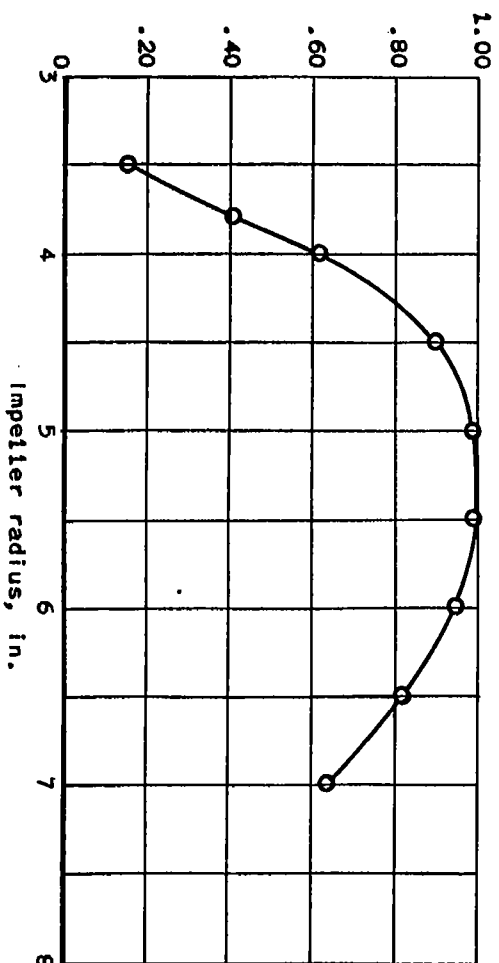
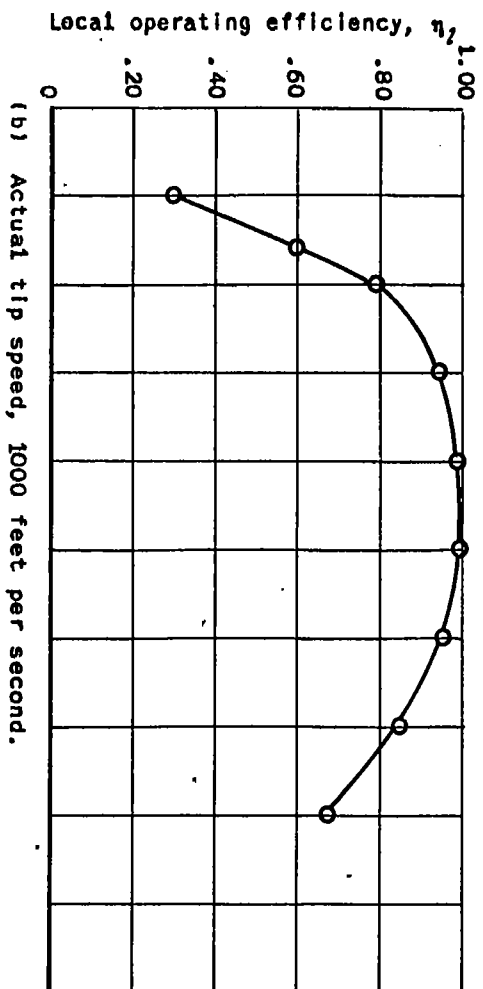
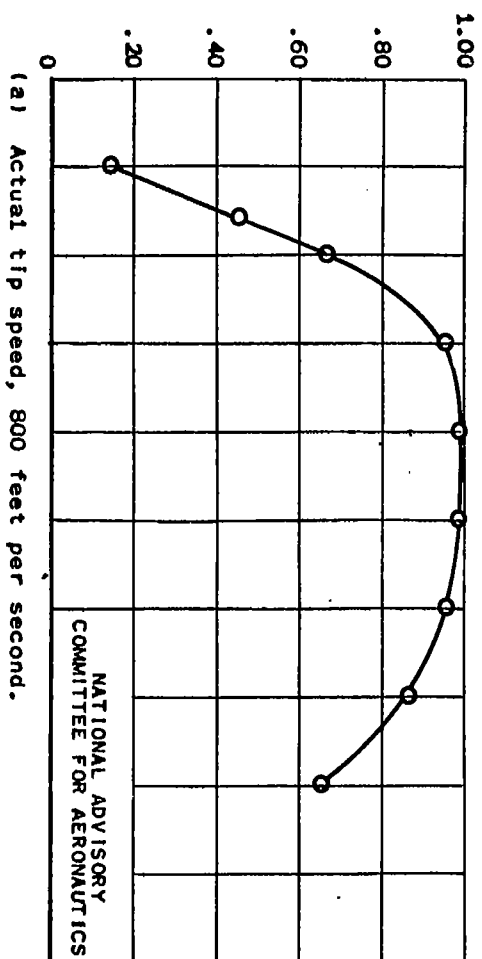


Figure 6. - Distribution of local operating efficiency of radial-inlet impeller along radius at peak-efficiency points.

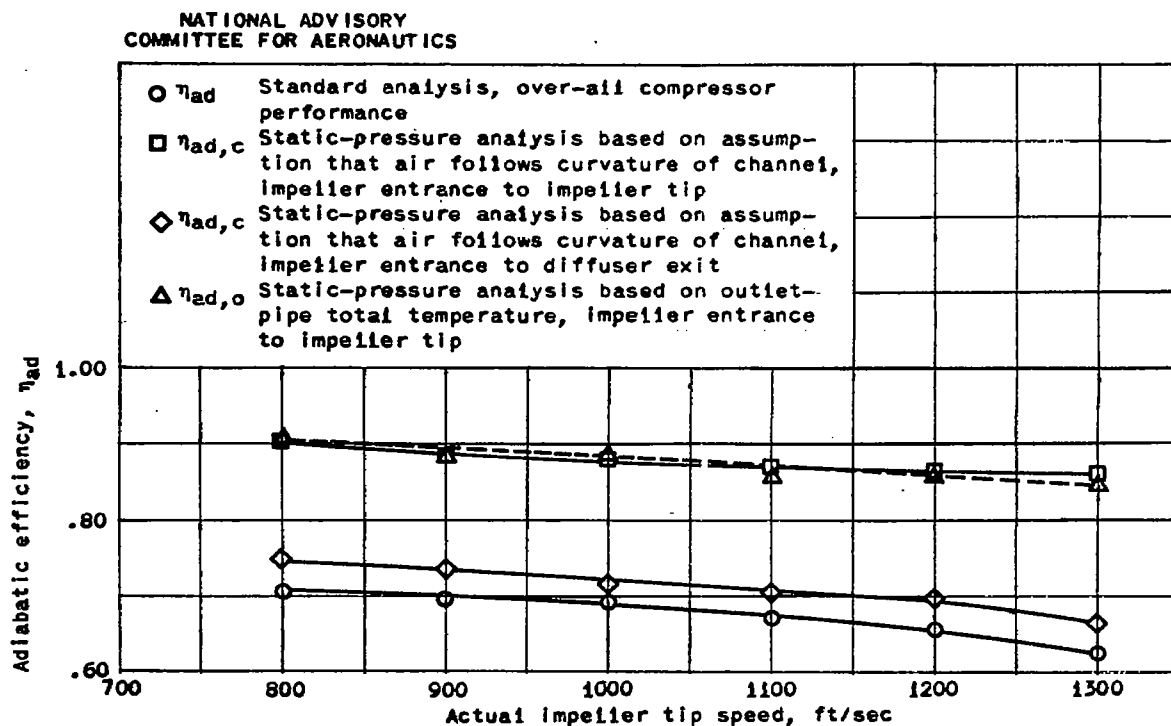


Figure 7. - Peak adiabatic compressor efficiency based on standard and static-pressure analyses for radial-inlet impeller and vaneless diffuser.

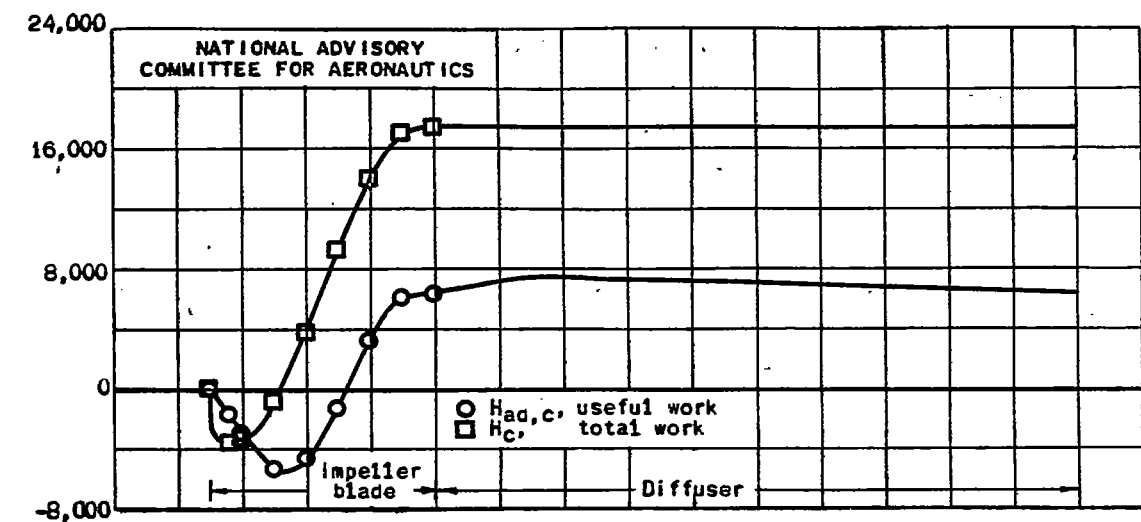
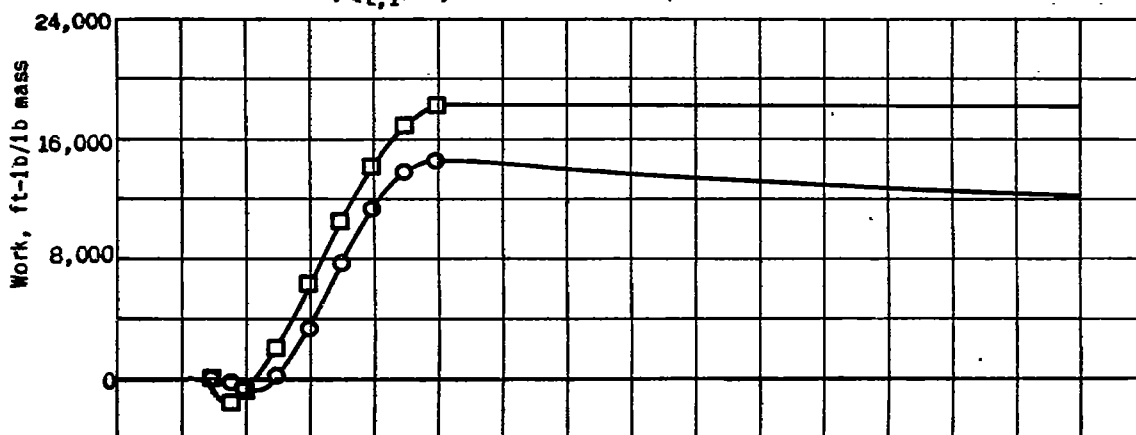
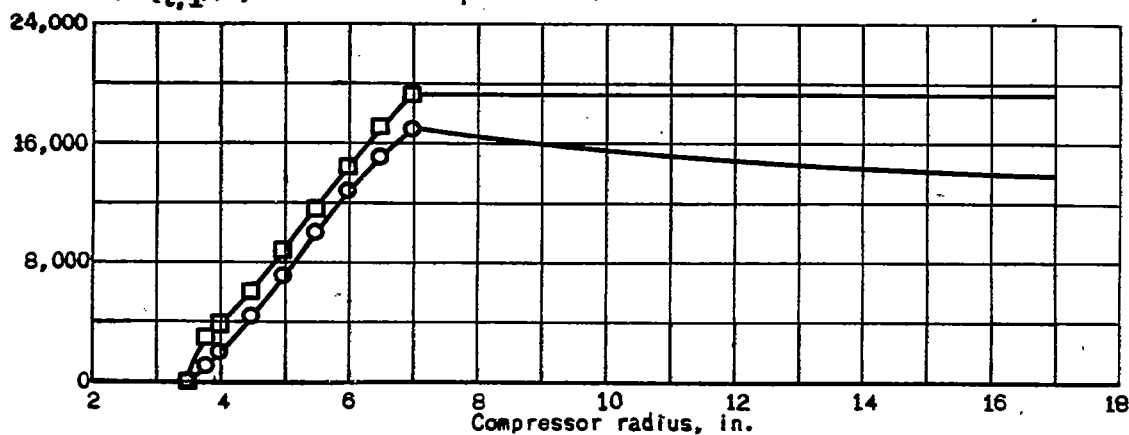
(a) Maximum flow,  $Q_{t,1}/\sqrt{\theta}$ , 4030 cubic feet per minute.(b)  $Q_{t,1}/\sqrt{\theta}$ , 3546 cubic feet per minute.(c) Minimum flow,  $Q_{t,1}/\sqrt{\theta}$ , 1448 cubic feet per minute.

Figure 8. - Distribution of useful work  $H_{ad,c}$  and total work  $H_c$  of compression along radius of radial-inlet impeller and vaneless diffuser at actual tip speed of 800 feet per second.

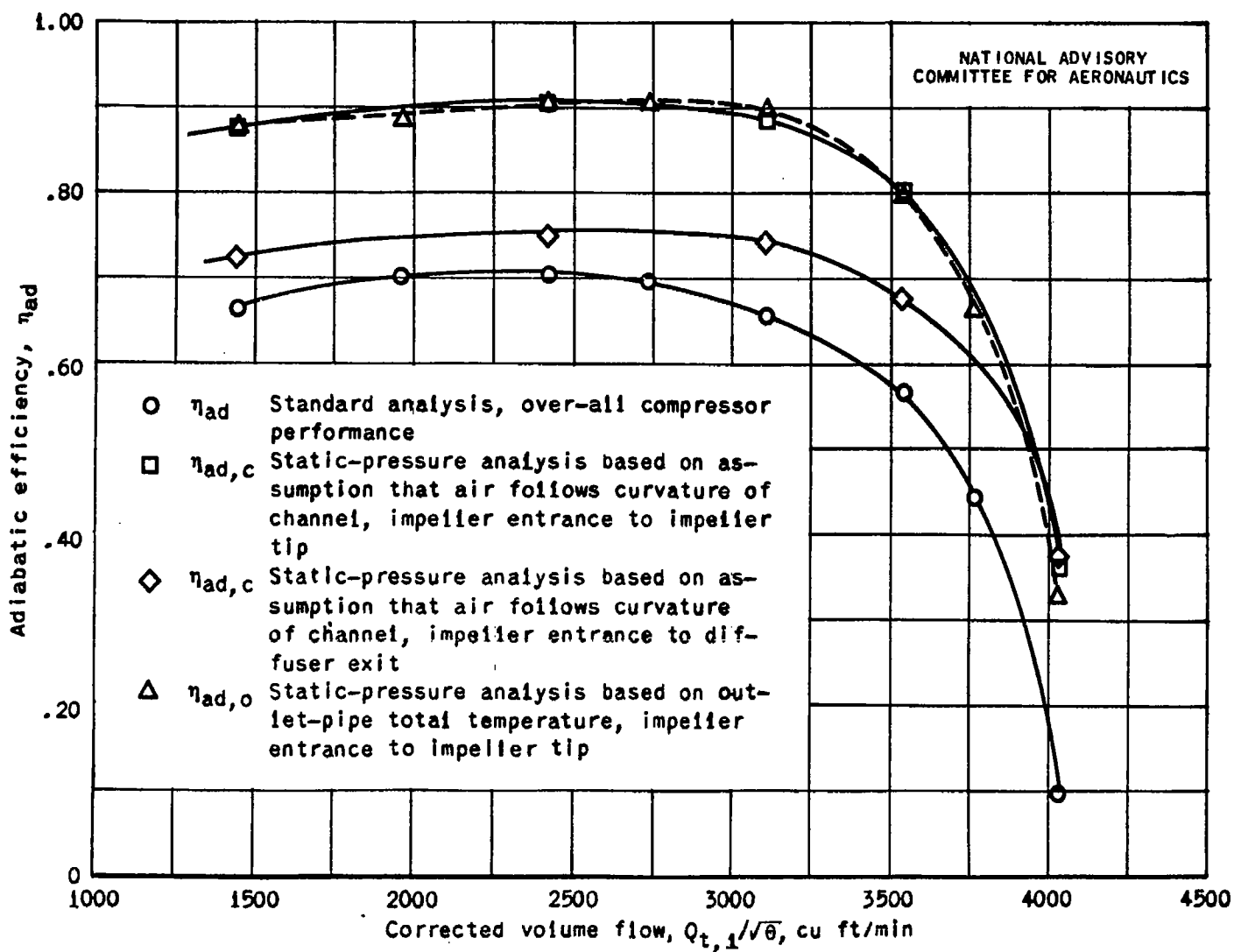


Figure 9. - Adiabatic efficiency based on standard and static-pressure analyses for radial-inlet impeller and vaneless diffuser at an actual tip speed of 800 feet per second.

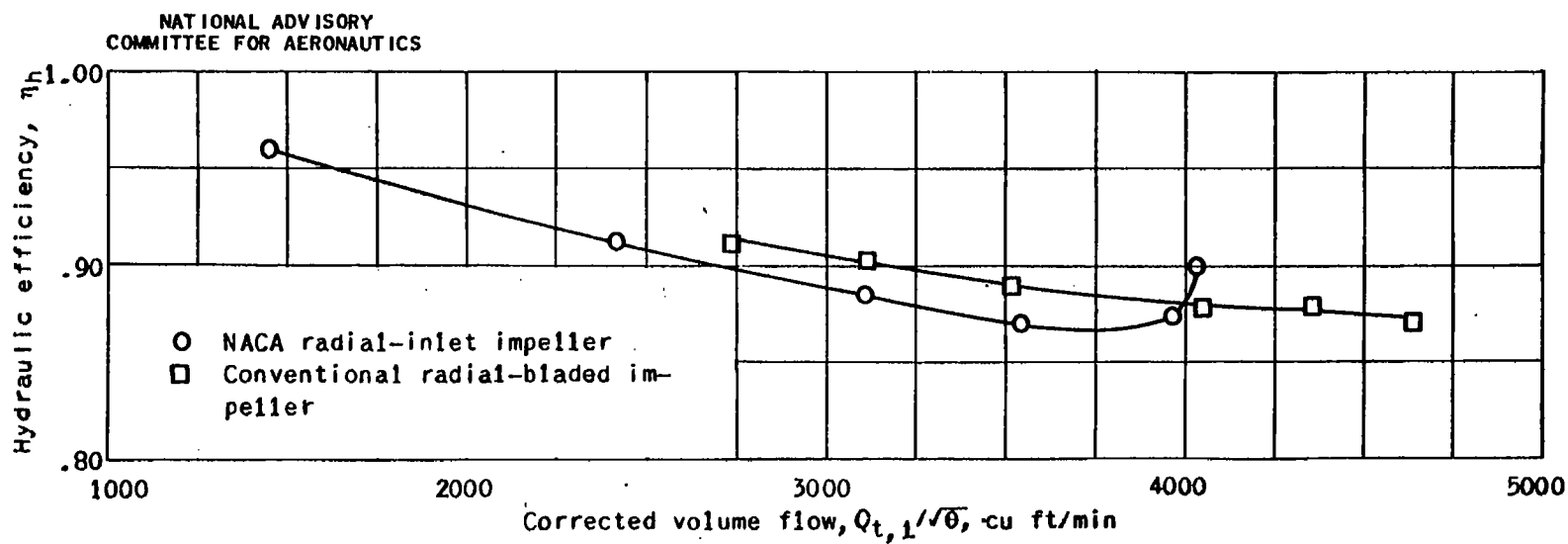
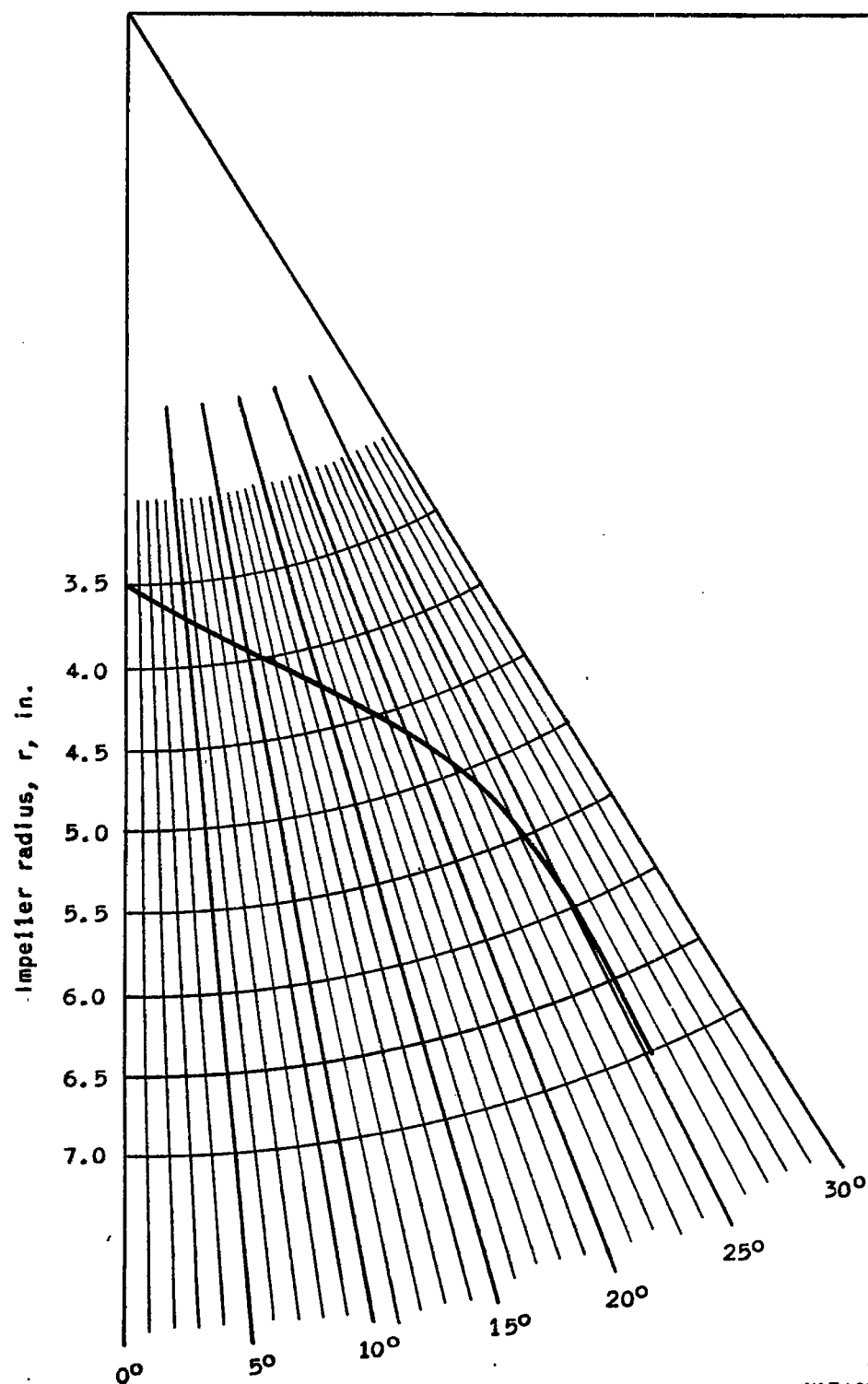
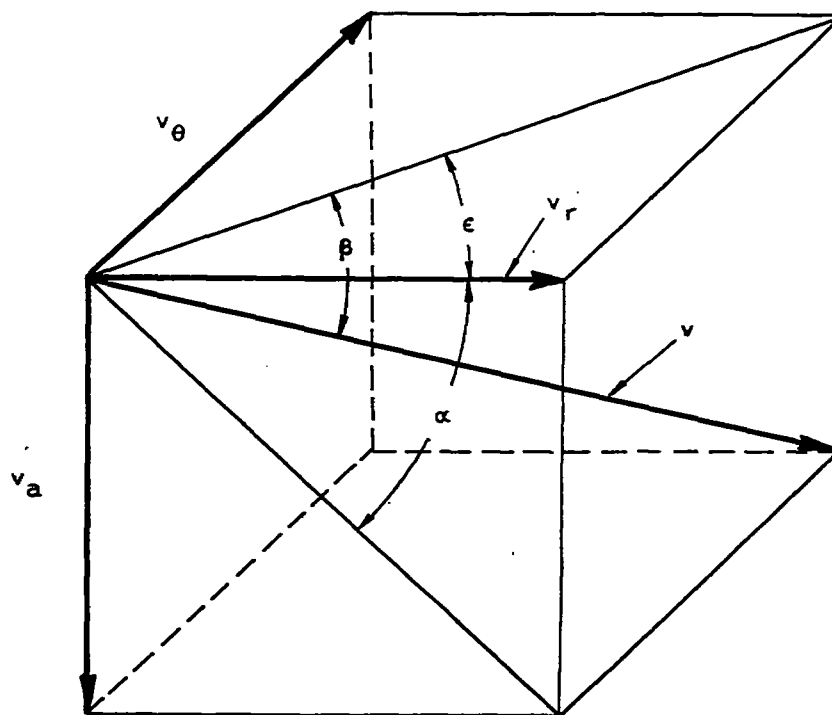


Figure 10. - Hydraulic efficiency of radial-inlet impeller and conventional impeller at an actual tip speed of 800 feet per second.



NATIONAL ADVISORY  
COMMITTEE FOR AERONAUTICS

Figure 11. - Blade shape of radial-inlet impeller.



$$\beta = \tan^{-1} \cos \epsilon \tan \alpha$$

$$v_a = v \sin \beta$$

$$v_\theta = v \sin \epsilon \cos \beta$$

$$v_r = v \cos \epsilon \cos \beta$$

NATIONAL ADVISORY  
COMMITTEE FOR AERONAUTICS

Figure 12. - Vector diagram of angular relations in impeller passage.

